Wolter-I-like X ray telescope structure using one conical mirror and one quadric mirror

Shenghao Chen (陈晟昊)[1,2], Shuang Ma (马 爽)[1,2], and Zhanshan Wang (王占山)[1,2,*]

[1]*Key Laboratory of Advanced Micro-Structure Materials, Ministry of Education, Shanghai 200092, China*
[2]*Institute of Precision Optical Engineering, School of Physics Science and Engineering, Tongji University, Shanghai 200092, China*
**Corresponding author: wangzs@tongji.edu.cn*

Received September 12, 2016; accepted October 28, 2016; posted online December 1, 2016

Nested multilayer mirrors are commonly used in X ray telescope structure to increase the collecting area. To balance the difficulty and cost of producing these mirrors, Wolter-I structures are replaced with conical Wolter-I structures, but these can lead to significantly poorer angular resolutions. In this Letter, we consider changing one of the mirror shapes (paraboloid or hyperboloid) of a Wolter-I structure to a conical mirror shape, while the other mirror shape remains a quadric surface-type structure, which can thus ensure the imaging quality. The cone-hyperboloid structure is nested to obtain on-axis angular resolution and off-axis images.

OCIS codes: 340.7740, 220.2740, 350.1260.
doi: 10.3788/COL201614.123401.

The telescope is an important observation device that has already produced numerous research results that have raised scientific awareness of the unknown universe[1–3]. Grazing incidence X ray telescopes are used to study X ray astronomy, which is a branch of astronomy related to the observation of X rays from astronomical objects.

Grazing incidence X ray telescope structures were pioneered by Wolter[4] in 1952, when he introduced a paraboloid-hyperboloid type 1 (Wolter-I) structure that consisted of a paraboloidal primary mirror and a confocal hyperboloidal secondary mirror. To increase the collecting area, Van Speybroeck and Chase[5] proposed the concept of a multilayer nested telescope in 1972. The nested Wolter-I X ray telescope is an important observation device with a very high angular resolution that is mounted on satellites, such as the Chandra X ray observatory[6–8] and the XMM-Newton[9–11]. This type of telescope can also focus on geometrical collection areas, but the fabrication of mirrors with required quadric surface is highly difficult.

On the basis of the Wolter-I structure, several different mirror shapes have been optimally designed for different purposes in the past. To ensure strict satisfaction of the Abbe sine condition, Wolter[12] proposed the Wolter–Schwarzschild structure in his second Letter, which exactly fulfilled the Abbe sine condition and thus eliminated the coma aberration for paraxial rays. Werner[13] designed several polynomials with a factor between 2 and 4 for X ray telescope structures that could improve the angular resolution. Conconi and Campana[14] and Burrows *et al.*[15] determined merit functions that were used to optimize the polynomials for large-field X ray imaging. Harvey *et al.*[16] designed a telescope with a hyperboloid–hyperboloid (HH) structure to optimize the angular resolution in the case of a large field of view. Petre[17] and Serlemitsos[18] designed cone–cone type-I telescope structures, called conical Wolter-I telescopes; these are widely used in actual applications, such as in Suzaku[19–21], NuSTAR[22–24], and Astro-H[25–27]. Saha and Zhang[28] simply added a second-order axial sag to optimize the on-axis image spot of the conical Wolter-I telescope. The conical Wolter-I telescope has a simple principle: it uses two conical mirrors to replace the paraboloidal and hyperboloidal surfaces. The most important advantage of this is that the difficulty and the cost of fabricating the mirrors both decrease dramatically, and thus, the geometrical collection area can be increased by the addition of more nested layers. However, the most serious problem with this structure is that the angular resolution is significantly worse. Most of these designs have not been adopted in practical applications, except the simple conical Wolter-I telescope, because the complicated mirror shapes make them difficult to fabricate and test. An X ray telescope structure should be designed with equal importance being given to increasing the geometrical collection area while ensuring the best possible angular resolution. At the same time, the difficulty, time, and cost of fabrication of the mirrors must also be considered.

In this Letter, we consider changing one of the mirror shapes of the Wolter-I structure to a conical mirror, which could reduce the production cost in comparison to that required for a paraboloid mirror or hyperboloid mirror. The other mirror shape would still have a quadric-type surface, which includes paraboloid, hyperboloid, and ellipse shapes, to ensure the imaging quality.

The designs of the cone-hyperboloid (CH), cone-paraboloid (CP), and cone-ellipse (CE) mirrors are discussed in this section. The positions of the mirrors can be calculated based on the Wolter-I telescope structure that is shown in a schematic diagram in Fig. 1[29]. F_1 is the focus of the paraboloid and the hyperboloid, and F_2 is the other focus of the hyperboloid. f is the focal length of the telescope. L is the axial length of each mirror.

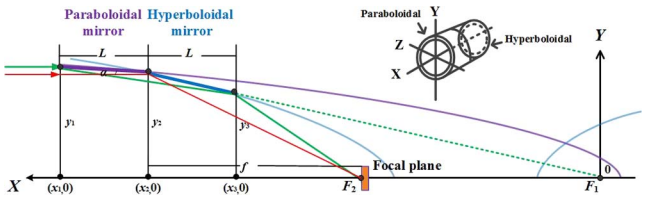

Fig. 1. Schematic diagram of the Wolter-I telescope used in the calculations.

(x_1, y_1) and (x_2, y_2) are the coordinates that determine the position of the primary mirror, while y_1 and y_2 are defined as the distance from the bottom location of the mirrors to the X-axis. (x_2, y_2) and (x_3, y_3) are the coordinates that determine the position of the secondary mirror.

A Wolter-I telescope can be completely defined based on three independent parameters: the paraboloid constant p, and the two hyperboloid constants, a and b. The parabolic and hyperbolic equations are set on the basis of the structure in Fig. 1 as

$$\text{Paraboloid } y^2 = p \cdot (2x + p), \tag{1}$$

$$\text{Hyperboloid } \frac{(x-c)^2}{a^2} - \frac{y^2}{b^2} = 1. \tag{2}$$

Similarly, an ellipse equation is set in Fig. 1 as

$$\text{Ellipse } \frac{(x-c)^2}{a^2} + \frac{y^2}{b^2} = 1. \tag{3}$$

The initial structure parameters of the telescope are the same as those of the XTP[30–32] (X ray timing and polarization) satellite. The telescope parameters are: focal length f of 4550 mm, telescope radius y_2 of 225 mm, and the axial length L and the thickness t of each mirror are 100 and 0.3 mm, respectively. Table 1 shows the positions of the Wolter-I mirrors in Fig. 1.

From Table 1, α is the angle of incidence of the rays on the surfaces, which are to be equal at the circle of intersection. By setting the telescope focus F_2 in Fig. 1 to be the focus of the quadric surface of the secondary mirrors, the functions of the three structures in this coordinate system can be described as follows:

$$\text{Hyperboloid } \frac{(x-c_{sh})^2}{a_{sh}^2} - \frac{y^2}{b_{sh}^2} = 1, \tag{4}$$

$$\text{Paraboloid } y^2 = 2p_s\left(x - x_2 + f + \frac{p_s}{2}\right), \tag{5}$$

Table 1. Parameters of the Wolter-I Structure

A (deg.)	x_1 (mm)	x_2 (mm)	x_3 (mm)	y_1 (mm)	y_2 (mm)	y_3 (mm)
0.7083	9198	9098	8998	226.233	225	221.332

$$\text{Ellipse } \frac{(x - x_2 + f - c_{se})^2}{a_{se}^2} + \frac{y^2}{b_{se}^2} = 1. \tag{6}$$

When the rays parallel to the optical axis are incident on the surface of the primary mirror (cone), the angles of incidence are the same with respect to the slope of the cone mirror k_c. However, the angles between the secondary light beams reflected by the quadric mirrors and the optical axis are quite different because of the different slopes at each point on the secondary mirrors. Figure 2 shows the optical path diagram for beams that are reflected by the quadric mirror. Δ is the spot size at the focal plane. When the values of y_1, y_2, and y_3 remain constant, the slope of the cone mirror is

$$k_c = (y_1 - y_2)/L. \tag{7}$$

The slopes k_n (k_2 and k_3) of the quadric mirrors are given by

$$\text{Hyperboloid } k_n = \frac{(x_n - c_{sh})}{y_n} \cdot \frac{b_{sh}^2}{a_{sh}^2}, \tag{8}$$

$$\text{Paraboloid } k_n = p_s/y_n, \tag{9}$$

$$\text{Ellipse } k_n = -\frac{(x_n - x_2 + f - c_{se})}{y_n} \cdot \frac{b_{se}^2}{a_{se}^2}. \tag{10}$$

In the cone-quadric structure, r_1 and r_2 are the actual vertical heights between the light spots and the optical axis at the focal plane:

$$r_1 = y_2 - y_2' = y_2 - f \cdot (2k_2 - 2k_c), \tag{11}$$

$$r_2 = y_3 - y_3' = y_3 - (f - L) \cdot (2k_3 - 2k_c). \tag{12}$$

Therefore, the value of the radius of spot $\Delta/2$ at the focal plane is the same as the larger of the values of r_1 and r_2.

The radius of the curve vertex R and the square of the curve eccentricity e^2 are calculated, respectively, by

$$R = b^2/a, \tag{13}$$

$$e^2 = c^2/a^2. \tag{14}$$

Equations (7)–(14) have been used to calculate the parameters of these structures, and the results are listed in Table 2.

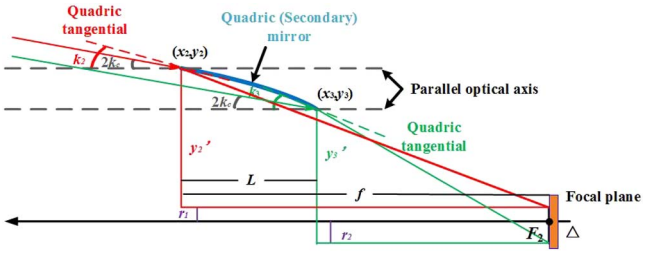

Fig. 2. Paths of X rays when reflected by the quadric mirror.

Table 2. Parameters of CH, CP, and CE Structures

	R (mm)	e^2	r_1 (mm)	r_2 (mm)	$\Delta/2$ (mm)
CH	−2.781	−1.001	0.502	−0.233	0.502
CP	−8.185	−1	6.152	1.928	6.152
CE	−12.476	−0.998	9.729	−1.670	9.729

$\Delta/2$ is the image radius by calculation. Similar results can be obtained via Zemax (a ray-tracing system) simulations, as shown in Fig. 3.

From Figs. 3(b) and 3(c), the images are defocused because of the changes in the structures. The image radii in the simulations are approximately the size of $\Delta/2$. We have optimized the focal lengths of these structures to obtain the best possible angular resolution, and the results are listed in Table 3.

Figure 4 shows the different images of the cone-quadric structure after the optimization process. From the calculated results of the simulations, we determined that the CH structure is particularly suitable for engineering applications, this also suggests that the CH structure will provide the best imaging quality.

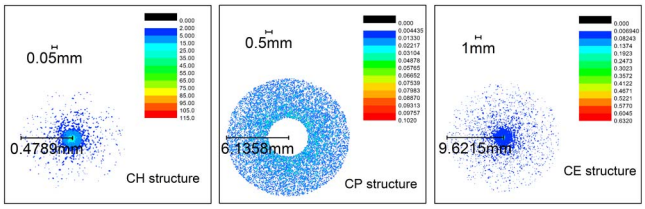

Fig. 3. Different images of cone-quadric structures produced by Zemax simulations. (a) CH structure, (b) CP structure, and (c) CE structure.

Table 3. Optimization of Parameters of CH, CP, and CE structures

Structure (mm)		CH	CP	CE
Before optimization	F	4550	4550	4550
	Radius of spot	0.479	6.136	9.622
After optimization	F change	−3.061	+83.853	+74.640
	Radius of spot	0.310	2.090	6.155

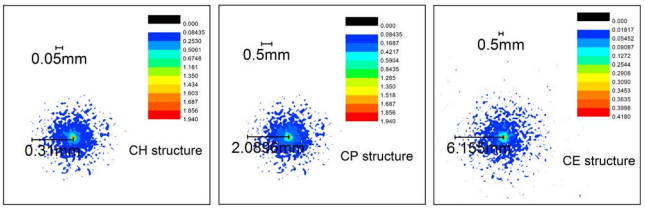

Fig. 4. Different images of cone-quadric structure after optimization. (a) CH structure, (b) CP structure, and (c) CE structure.

The quadric-cone (including PC, HC, and EC) structure is designed in this section. Where the telescope focus F_1 was set as the focus of the quadric surface of the primary mirrors. The functions of the three structures in this coordinate system could then be described as follows:

$$\text{Paraboloid } y^2 = p_p(2x + p_p), \tag{15}$$

$$\text{Hyperboloid } \frac{(x + c_{ph})^2}{a_{ph}^2} - \frac{y^2}{b_{ph}^2} = 1, \tag{16}$$

$$\text{Ellipse } \frac{(x - c_{pe})^2}{a_{pe}^2} + \frac{y^2}{b_{pe}^2} = 1. \tag{17}$$

Equations (15)–(17) have been used to calculate these parameters, and the results are listed in Table 4.

The results from the hyperboloid function are the same as those for the paraboloid, and there is no real number for the ellipse function. So, we could only simulate the PC structure; the resulting image is shown in Fig. 5.

Obvious defocusing is also shown in Fig. 5. We have subsequently optimized the focal lengths of the structure to obtain the best possible angular resolution. The resulting parameters are listed in Table 5, and the resulting

Table 4. Parameters of PC, HC, and EC Structures

	p (mm)	a (mm)	B (mm)	c (mm)	e^2	R (mm)
PC	−2.782				1	2.782
HC		4.946×10^{16}	3.709×10^{8}	4.946×10^{16}	1	2.782
EC		4.946×10^{16}	-3.709×10^{8}i	-4.946×10^{16}	1	2.782

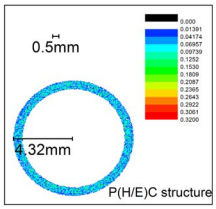

Fig. 5. Image of quadric cone.

Table 5. Optimization of PC Structure

Before Optimization		After Optimization	
Focal length (mm)	4550	Focal length change (mm)	+81.037
Radius of spot (mm)	4.322	Radius of spot (mm)	0.359

image is shown in Fig. 6. The spot radius of the PC structure is similar to that of the CH structure after optimization. In contrast, however, the optimal focus value of this structure is positive in that the system has a longer focal length, which is undesired result that wastes materials and increases the difficulty of manipulating the satellite. A comparison of the cone-quadric and quadric-cone structures shows that the CH structure produces the best image quality and optimal focusing.

The nested structure is thus designed as shown in Fig. 7[5]. To increase the geometrical collection areas to a maximum under the same telescope diameter, the inner surfaces should be sufficiently small to allow all axial rays that strike the next outer surface to pass. Δr is defined to be the distance between the bottom location of the upper layer and the top location of the lower layer. i is the outermost layer of the nested structure, and $i-1$ is the inside adjacent layer to the outermost layer. The relationship between y and t is given by

$$y_{1,i-1} = y_{2,i} - t. \tag{18}$$

When the thickness $t = 0.3$ mm of the mirrors is known and $f = 4550$ mm, $L = 100$ mm, and $y_{2,i} = 225$ mm, the positions and structural parameters of each layer of mirrors can be calculated individually.

A 10-layer nested CH structure is simulated using Zemax, and the resulting image is shown in Fig. 8. The central dotted circle denotes the half-power diameter (HPD), and the spot radius of the HPD is approximately 0.135 mm. The angular resolution of the CH structured telescope is thus approximately 12.24 arcsec (HPD).

Under the same nested conditions, the on-axis ideal angular resolution of the Wolter-I (PH) structure telescope is approximately 0.00 arcsec (HPD), and the

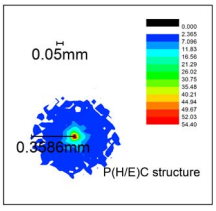

Fig. 6. Image of quadric cone after optimization.

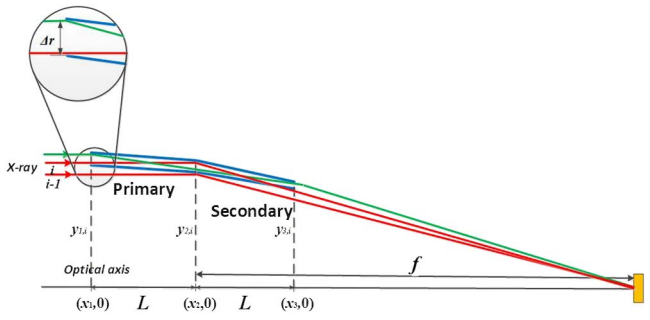

Fig. 7. Nested structure of the Wolter-I telescope.

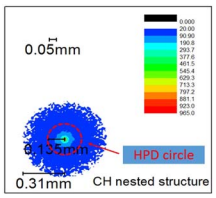

Fig. 8. Image of CH nested structure.

angular resolution of the conical Wolter-I (CC) telescope is approximately 28.58 arcsec (HPD).

Table 6 shows the spot diagrams of three types of nested structures on different fields of view at a flat plane, which has the best angular resolution on-axis.

For a conical Wolter-I structure, in a flat focal plane whose axial location is defined by the axial ray focus, the image size (HPD) remains virtually unchanged as a function of the off-axis angle within the mirror's field of view[17,20]. We found the same rule applies to the CH structure. There are some optimum focal planes, which can be approximated by a hyperboloid, as determined for each field angle in theory[29]. So we got the best angular resolutions at different optimum focal planes for a CH nested structure, too. Figure 9 shows the changes in resolution (HPD) as the off-axis angles change.

We set up the same number of incident rays as the different structures. The rays that are collected from the detector are used to describe the geometrical collection area[32]. Figure 10 shows the change in the geometrical collection area with the off-axis angle.

In conclusion, we consider some new Wolter-I-like X ray telescope structures that use one conical mirror and one quadric mirror. After comparing and analyzing these structures, the optimum structure is judged to be the CH structure. The results show that the angular resolution of the CH nested structure is approximately 12.24 arcsec (HPD), which is obviously better than the

Table 6. Spot Diagrams of Three Types of Nested Structures from Different Fields of View

FOV (arcmin)	PH structure	CC structure	CH structure
0			
5			
10		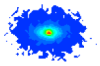	
15		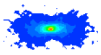	
20			

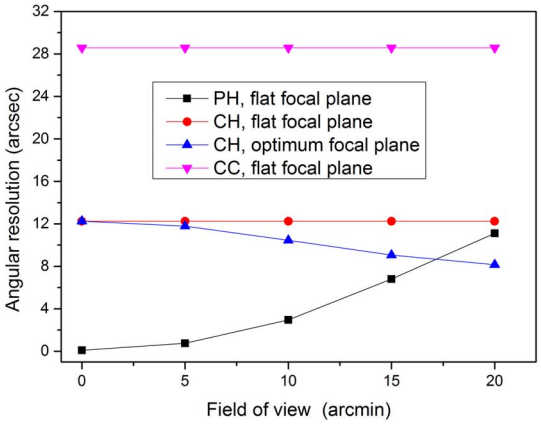

Fig. 9. Changes in angular resolution (HPD) with changes in the field of view.

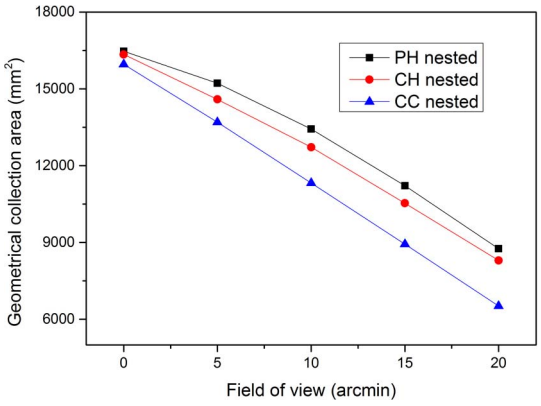

Fig. 10. Changes in geometrical collection area with changes in the field of view.

28.58 arcsec of the CC nest structure, and images of the CH nested structure are shown from different fields of view. Therefore, the CH nested structure is selected as a reasonable choice to use in the next stage of our research.

This work was supported by the National Science Instrument and Equipment Development Major Project of Ministry of Science and Technology of China (Nos. 2012YQ24026402 and 2012YQ04016403) and the Youth Science Fund Project of the National Natural Science Fund of China (No. 11505129).

References

1. E. Hand, Science **352**, 1155 (2016).
2. Z. Li, H. Lu, and X. Yuan, Chin. Opt. Lett. **13**, 111101 (2015).
3. C. Rao, L. Zhu, X. Rao, L. Zhang, H. Bao, L. Kong, Y. Guo, X. Ma, M. Li, C. Wang, X. Zhang, X. Fan, D. Chen, Z. Feng, X. Wang, N. Gu, and Z. Wang, Chin. Opt. Lett. **13**, 120101 (2015).
4. H. Wolter, Ann. Phys. **445**, 94 (1952).
5. L. P. Van Speybroeck and R. C. Chase, Appl. Opt. **11**, 440 (1972).
6. M. C. Weisskopf, S. L. O'Dell, R. F. Eisneret, and L. P. Van Speybroeck, Proc. SPIE **2515**, 312 (1995).
7. T. J. Gaetz, W. A. Podgorski, L. M. Cohen, M. D. Freeman, R. J. Edgar, D. Jerius, L. Van Speybroeck, P. Zhao, J. Kolodziejczak, and M. Weisskopf, Proc. SPIE **3113**, 77 (1997).
8. S. L. O'Dell and M. C. Weisskopf, Proc. SPIE **344**, 708 (1998).
9. P. L. Jensen, J. M. Ellwood, and A. Peacock, Proc. SPIE **1160**, 525 (1989).
10. O. Citterio, P. Conconi, M. Ghigo, F. Mazzoleni, H. W. Heinrich, W. Burkert, N. Schulz, P. Gondoin, K. Van Katwijk, and R. J. Laurance, Proc. SPIE **1742**, 256 (1992).
11. D. H. Lumb, F. A. Jansen, and N. Schartel, Opt. Eng. **51**, 011009 (2012).
12. H. Wolter, Ann. Phys. **445**, 286 (1952).
13. W. Werner, Appl. Opt. **16**, 764 (1977).
14. P. Conconi and S. Campana, Astron. Astrophys. **372**, 1088 (2001).
15. C. J. Burrows, R. Burg, and R. Giacconi, Astrophys. J. **392**, 760 (1992).
16. J. E. Harvey, A. Krywonos, P. L. Thomoson, and T. T. Saha, Appl. Opt. **40**, 136 (2001).
17. R. Petre and P. J. Serlemitsos, Appl. Opt. **24**, 1833 (1985).
18. P. J. Serlemitsos, Appl. Opt. **27**, 1447 (1988).
19. H. Kunieda, M. Ishida, T. Endo, Y. Hidaka, H. Honda, K. Imamura, J. Ishida, M. Maeda, K. Misaki, R. Shibata, A. Furuzawa, K. Haga, Y. Ogasaka, T. Okajima, Y. Tawara, Y. Terashima, M. Watanabe, K. Yamashita, T. Yoshioka, P. J. Serlemitsos, Y. Soong, and K. W. Chan, Appl. Opt. **40**, 553 (2001).
20. R. Shibata, M. Ishida, H. Kunieda, T. Endo, H. Honda, K. Misaki, J. Ishida, K. Imamura, Y. Hidaka, M. Maeda, Y. Tawara, Y. Ogasaka, A. Furuzawa, M. Watanabe, Y. Terashima, T. Yoshioka, T. Okajima, K. Yamashita, P. J. Serlemitsos, Y. Soong, and K. W. Chan, Appl. Opt. **40**, 3762 (2001).
21. K. Misaki, Y. Hidaka, M. Ishida, R. Shibata, A. Furuzawa, Y. Haba, K. Itoh, H. Mori, and H. Kunieda, Appl. Opt. **44**, 916 (2005).
22. J. E. Koglin, C. M. Hubert Chen, J. C. Chonko, F. E. Christensen, W. W. Craig, T. R. Decker, C. J. Hailey, F. A. Harrison, C. P. Jensen, K. K. Madsen, M. J. Pivovaroff, M. Stern, D. L. Windt, and E. Ziegler, Proc. SPIE **46**, 5488 (2004).
23. J. E. Koglin, F. E. Christensen, W. W. Craig, T. R. Decker, C. J. Hailey, F. A. Harrison, C. Hawthorn, C. P. Jensen, K. K. Madsen, M. Stern, G. Tajiri, and M. D. Taylor, Proc. SPIE **5900**, 59000X (2005).
24. N. J. Westergaard, K. K. Madsen, N. F. Brejnholt, J. E. Koglin, F. E. Christensen, M. J. Pivovaroff, and J. K. Vogel, Proc. SPIE **8443**, 84431X (2012).
25. T. Takahashi, K. Mitsuda, and H. Kunieda, and the NeXT team, Proc. SPIE **6266**, 62660D (2006).
26. Y. Tawara, Adv. Space Res. **40**, 1289 (2007).
27. A. Furuzawa, Y. Ogasaka, H. Kunieda, T. Miyazawa, M. Sakai, Y. Kinoshita, Y. Makinae, S. Sasaya, Y. Kanou, D. Niki, T. Ohgi, N. Oishi, K. Yamane, N. Yamane, Y. Ishida, Y. Haba, Y. Tawara, K. Yamashita, M. Ishida, Y. Maeda, H. Mori, K. Tamura, H. Awaki, and T. Okajima, Proc. SPIE **7437**, 743709 (2010).
28. T. T. Saha and W. Zhang, Appl. Opt. **42**, 4599 (2003).
29. J. D. Mangus and J. H. Underwood, Appl. Opt. **8**, 95 (1969).
30. Q. Huang, J. Zhang, R. Qi, Y. Yan, F. Wang, J. Zhu, Z. Zhang, and Z. Wang, Opt. Express **24**, 15620 (2016).
31. B. Mu, H. Liu, H. Jin, X. Yan, F. Wang, W. Li, H. Chen, and Z. Wang, Chin. Opt. Lett. **10**, 103401 (2012).
32. S. Chen, B. Mu, S. Ma, and Z. Wang, Proc. SPIE **9272**, 92721R (2014).